Vibrational properties of $Ca_3Sc_2Ge_3O_{12}$, a garnet host crystal for laser applications

2000 J. Phys.: Condens. Matter 12 4665

(http://iopscience.iop.org/0953-8984/12/21/310)

J. Phys.: Condens. Matter **12** (2000) 4665–4674. Printed in the UK PII: S0953-8984(00)08910-4

Vibrational properties of $Ca_3Sc_2Ge_3O_{12}$, a garnet host crystal for laser applications

Enrico Cavalli†‖, Ester Zannoni†, Marco Bettinelli‡, Adolfo Speghini‡, Mauro Tonelli§ and Alessandra Toncelli§

† Dipartimento di Chimica Generale ed Inorganica, Chimica Analitica e Chimica Fisica, Università di Parma - Viale delle Scienze 17/a, 43100 Parma, Italy
‡ Dipartimento Scientifico e Tecnologico, Università di Verona Ca' Vignal - Strada Le Grazie 15, 37134 Verona, Italy
§ INFM and Dipartimento di Fisica, Università di Pisa - Via Buonarroti 2, 56127 Pisa, Italy

E-mail: cavalli@ipruniv.cce.unipr.it

Received 25 October 1999, in final form 14 March 2000

Abstract. The IR and the Raman spectra of the $Ca_3Sc_2Ge_3O_{12}$ (CaSGG) garnet crystal have been measured and discussed in terms of internal and external modes of the tetrahedral GeO_4^{4-} moiety. Some important aspects of the electronic spectroscopy of these materials activated with luminescent ions, i.e. the multiphonon relaxation of the excited states and the vibrational structure of the optical bands, have been taken into consideration, and correspondences with the vibrational properties of the host lattice have been presented.

1. Introduction

In a series of recent papers [1–4], we have demonstrated that $Ca_3Sc_2Ge_3O_{12}$ (CaSGG) garnet crystals doped with suitable luminescent species are attractive materials for solid-state laser applications. It is well known that the optical properties of an active ion located at a lattice site of a crystal strongly depend on the electron–phonon interactions of the impurity ions. The knowledge of the vibrational properties of a host matrix is then expected to be useful in order to understand the aspects of the optical spectroscopy of luminescent materials which depend on the ion-lattice interactions. In this work we present, for the first time to our knowledge, the IR and Raman spectra of the CaSGG host lattice and discuss them on the basis of models described in previous papers. Moreover, we take into consideration two fundamental aspects of the optical properties of activated crystals, i.e. the multiphonon relaxation of the excited states and the vibrational structure of the absorption and emission bands, and discuss, for some suitably doped CaSGG crystals, the correspondences with the observed vibrational properties.

2. Experimental details

Pure or suitably doped crystals of CaSGG were grown by means of the 'flux growth' technique, using pure $CaCO_3$, Sc_2O_3 and GeO_2 as starting materials and Bi_2O_3–B_2O_3 as a solvent in the temperature range 1230–860 °C [5]. The average size of the crystals was about $3 \times 2 \times 2$ mm^3; their optical quality was good.

‖ Author to whom all correspondence should be addressed.

0953-8984/00/214665+10$30.00

Medium-infrared (MIR, from 550 to 900 cm^{-1}) and far-infrared (FIR, from 80 to 550 cm^{-1}) spectra were measured at room temperature using a Nicolet Magna 760 FTIR spectrometer. For the MIR range, an appropriate amount of the sample (about 3 wt%) was ground with dry KBr, the powder was pelletized and the absorption spectrum of the pellet was collected. In the FIR range, the sample (about 5 wt%) was carefully mixed with high-density polyethylene (HDPE) and the diffuse reflectance spectrum was measured, using pure HDPE as a reference.

The Raman measurements were carried out on a small, optically-polished single crystal. The 488.0 nm line of a Spectra-Physics Stabilite 2017 argon laser was used to obtain room-temperature Raman spectra. A fibre-optic probe coupled to a Dilor Superhead, equipped with a suitable notch filter, was employed. The scattered signal was analysed by a Jobin–Yvon HR460 monochromator and a CCD detector. Spectra were collected using a 1200 lines mm^{-1} grating with a spectral resolution of about 1 cm^{-1}.

The experimental set-up for the measurement of the absorption and emission spectra in the visible range has previously been described [2, 3].

3. Vibrational spectra: results and discussion

CaSGG has a garnet structure and belongs to the cubic crystallographic system. Its space group is $Ia3d$ (O_h^{10}), with cell parameter $a = 12.512$ Å and $Z = 8$ in the body-centred Bravais cell [5]. The 24 Ca^{2+} ions are located at the dodecahedral sites of the garnet lattice with D_2 real point symmetry, the 16 Sc^{3+} ions occupy distorted octahedral sites with C_{3i} actual point symmetry and the 24 Ge^{4+} ions lie at the distorted tetrahedral sites with S_4 point symmetry. The garnet structure can be described as a net of ScO_6 octahedra and GeO_4 tetrahedra linked through the corners; the polyhedra form chains along the three crystallographic directions in such a way that the cavities among them constitute the dodecahedral host sites occupied by the Ca^{2+} ions. Alternatively, the structure can be seen as the spatial development of moduli composed of a dodecahedral unit sharing four edges with as many other dodecahedra, the voids among them describing the octahedral and tetrahedral cavities occupied by the Sc^{3+} and Ge^{4+} ions, respectively. Each dodecahedron then shares edges with four other dodecahedra, four octahedra and two tetrahedra. It is then evident that the vibrations of the polyhedra are strongly coupled one to another.

The factor group analysis of the garnet lattice has already been carried out by Hurrell *et al* [6]; here we report only the final results that are essential to discuss our experimental data. First of all, the analysis is made easier if we consider a primitive cell instead of the conventional body-centred cell. In fact, the former contains only four formula units (80 atoms) and possesses the same symmetry elements of the factor group.

The 240 degrees of freedom of the unit cell give rise to a representation Γ of the O_h factor group, which can be reduced as

$$\Gamma = 3A_{1g} + 5A_{2g} + 8E_g + 14T_{1g} + 14T_{2g} + 5A_{1u} + 5A_{2u} + 10E_u + 18T_{1u} + 16T_{2u}.$$

The symmetry selection rules indicate that the T_{1u} modes are IR active and the A_{1g}, E_g and T_{2g} modes are Raman active. Moreover, one of the 18 T_{1u} modes concerns translational motions, and then will be IR inactive. In conclusion, we should observe, at most, 17 vibrational modes in the IR spectrum and 25 modes in the Raman spectrum.

3.1. IR spectra

The MIR and FIR spectra of CaSGG are shown in figures 1(a) and 1(b), respectively. They are composed of three band systems in the 100–200, 230–530 and 550–900 cm^{-1} regions,

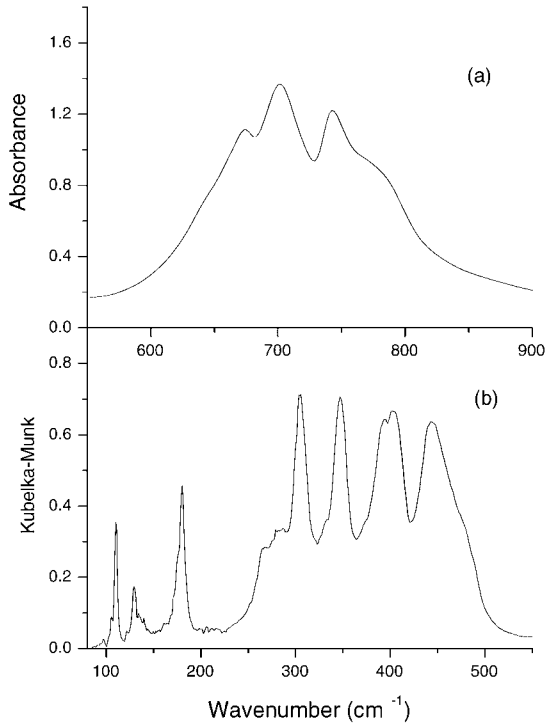

Figure 1. Room-temperature IR absorption spectrum of CaSGG: (a) MIR range, (b) FIR range.

respectively. The energies of the observed bands are reported in table 1. The degeneracy of the IR-active modes is partially removed under the influence of long-range electrostatic forces with each mode giving rise to a singly-degenerate longitudinal vibration (LO) and a doubly-degenerate transverse vibration (TO) [6]. The frequencies of the TO and LO T_{1u} modes could be determined from a Kramers–Kronig analysis of a normal reflectance spectrum in the IR range. Unfortunately, the size of the CaSGG crystals is too small to obtain a good-quality reflectance spectrum and for this reason we could not adopt the the procedure employed by Hurrell *et al* [6]. In any case, we remark that the TO–LO splitting should not be very important (see for instance [6] for YAG). Based on these considerations, at least 13 of the 17 T_{1u} modes could be identified.

The interpretation of the vibrational spectra of garnet crystals was a matter of discussion in some papers published at the end of the 1960s, and it is still, today, a problem to be solved. In particular, there is no agreement in the assignment of the bands in terms of local modes. For example, McDevitt [7] carefully examined the behaviour of the most intense absorption feature in the high-energy band system, and concluded that it is connected to the motions of the oxygen anions associated to the dodecahedral units. In contrast, Tarte [8] assigned the high-frequency bands to modes of the tetrahedral units whereas Hurrell *et al* [6] stated that these bands correspond to molecular modes, but they were not able to decide with certainty whether these are modes of the octahedral or of the tetrahedral units. In our opinion this uncertainty could be related to the great compactness of the garnet structure, which implies that the vibrations of the different polyhedra are strongly coupled to one another. We have also recorded the IR spectra of garnets with general formula $A_3B_2Ge_3O_{12}$, where A = Ca or Cd and B = Al, Ga or Cr and we have observed that the bands in the 550–900 cm^{-1} range do

Table 1. Frequencies and assignments of the bands observed in the IR and Raman spectra of CaSGG. A weak peak is denoted by w and a shoulder is denoted by sh.

ν_{IR} (cm^{-1})	Assignment	ν_{Raman} (cm^{-1})		Assignment
97.0 ± 0.5	lattice	133 ± 1 (w)		lattice
110.0 ± 0.5		169 ± 1		
129.5 ± 0.5				
~176 (sh)		267 ± 1		ν_2, ν_4
180.5 ± 0.5		295 ± 1		
		330 ± 1		
270.0 ± 0.5	ν_4	402 ± 1		
284.5 ± 0.5		468 ± 1	(A_{1g})	
305.5 ± 0.5		500 ± 1 (w)		
347.0 ± 0.5				
394.5 ± 0.5		688 ± 1		ν_1, ν_3
402.0 ± 0.5		~705 (w)		
442.5 ± 0.5		730 ± 1		
~478 (sh)		804 ± 1	(A_{1g})	
		~830 (w, sh)		
675.0 ± 0.5	ν_3			
702.0 ± 0.5				
742.5 ± 0.5				
~783 (sh)				

not vary much on passing from one compound to another. For this reason we think that the hypothesis of Tarte is at least reasonable, also considering that the Ge–O bond of the tetrahedral group is the one characterized by a higher degree of covalent character and therefore its force constant has to be higher with respect to the other molecular units. We therefore assign the bands in the 550–900 cm^{-1} range to the asymmetric stretching $\nu_3(T_2)$ transition allowed in tetrahedral symmetry. This mode splits into two components, E and B, on passing from the T_d to the S_4 symmetry, i.e. the site group symmetry of the GeO_4^{4-} unit. By taking into account the interactions with the lattice, these modes give rise to two factor group representations, each of them containing one or two IR-allowed (T_{1u}) components (see table IV of [6]). This accounts for the observed splitting of the high-energy band.

Similarly, the band system lying in the region 230–530 cm^{-1} can be assigned to the second mode IR-allowed in T_d symmetry, i.e. the bending mode $\nu_4(T_2)$. However, in this case the structure of the band is more complicated than for the case discussed above, probably due to the strong mixing between internal and external modes, as outlined by Hurrell *et al* [6] and McDevitt [7]. Concerning the bands in the 100–200 cm^{-1} region, all the authors agree on the assignment to lattice modes.

3.2. Raman spectra

The room-temperature Raman spectrum of CaSGG in the 100–900 cm^{-1} region is shown in figure 2. Only 13 of the 25 active modes are observed (see table 1). The Raman bands corresponding to totally symmetric A_{1g} modes at 468 and 804 cm^{-1} were easily identified as they are completely polarized irrespective of the orientation of the crystal axes with respect to the macroscopic axes. Hurrell *et al* [6] were able to assign only the symmetries of the normal modes observed in the Raman spectrum of YAG, whereas Koningstein and Sonnich Mortensen [9] proposed a site group analysis and the assignment in terms of external and internal modes of the tetrahedral MO_4^{n-} (S_4) groups. As in the case of the IR spectrum, we adopt this type of

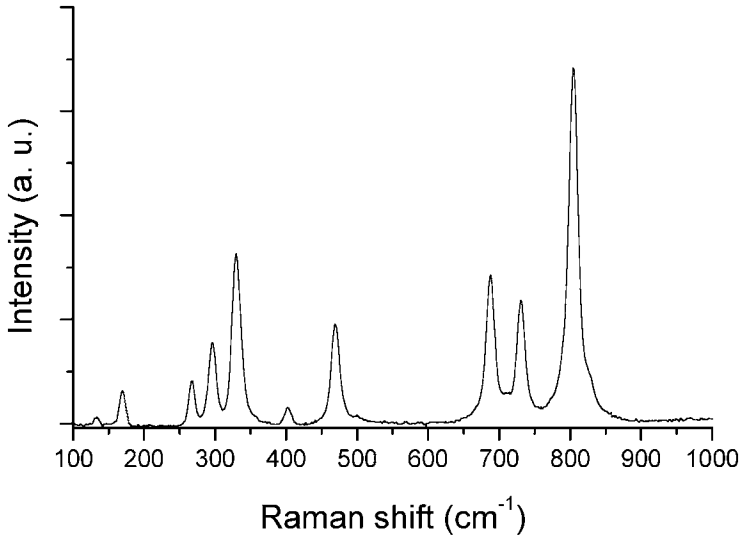

Figure 2. Room-temperature Raman spectrum of CaSGG.

model. The Raman spectrum can then be interpreted by considering the following guidelines [6, 10]:

- in regular T_d symmetry, all the four normal modes $\nu_1(A_1)$, $\nu_2(E)$, $\nu_3(T_2)$ and $\nu_4(T_2)$ are Raman active;
- the frequencies of the stretching modes (ν_1, ν_3) are higher than those of the bending modes (ν_2, ν_4);
- only the factor group representations corresponding to the ν_1 and ν_2 modes contain total-symmetric terms;
- each ν_n ($n = 1$–4) mode of the regular tetrahedral unit gives rise to a factor group representation containing two Raman-active (i.e. A_{1g}, E_g or T_{2g}) components (see table IV of [6]).

These statements help us in assigning the most intense features observed in the Raman spectrum. The results are reported in table 1. The data reported, as well as the proposed assignment, are more than sufficient to account for the interactions between the vibrational and electronic properties discussed in the following section.

4. The interaction between vibrational and electronic properties

4.1. Multiphonon relaxation of excited states of Ln^{3+} ions: the case of $^4F_{9/2}$ of Er^{3+} in CaSGG

The rate of depopulation of an excited state can be expressed as the sum of two contributions connected to the radiative and non-radiative processes [11]:

$$W = W_R + W_{NR}. \tag{1}$$

This well known relation is the starting point for the analysis of the decay of excited states of Ln^{3+} ions. The radiative transition probability W_R is, in principle, independent of the temperature, and can be evaluated from the Judd–Ofelt analysis of the room-temperature

absorption spectra [12–14]. In contrast, the non-radiative transition term W_{NR} takes into consideration all the mechanisms decreasing the efficiency of a given emission channel, and can be temperature dependent. Many different processes can contribute to W_{NR}: multiphonon relaxation, energy transfer processes, up-conversion and so on. Often many of them occur simultaneously and any tentative of analysis becomes difficult. Moreover, there are cases where only a single mechanism is active and the analysis of the temperature dependence of the lifetimes can yield useful information. The multiphonon relaxation is probably the best known and certainly the most common among these cases, and its temperature dependence is relatively simple. In fact, in the case of a transition between states belonging to a $4f^n$ configuration, the temperature dependence of W_{NR} is given by

$$W_{NR}(\mathrm{T}) = W_{NR}^{(0)}(1 + n_{eff})^p \tag{2}$$

where n_{eff} is the occupancy of the effective phonon modes:

$$n_{eff} = [\exp(\hbar\omega_{eff}/kT) - 1]^{-1} \tag{3}$$

and p is the number of phonons necessary to bridge the energy gap between the emitting and the final state. Equation (2) can be used for the best fit of the experimental values of the non-radiative transition probabilities obtained from the experimental measurements of the lifetimes and calculated using (1). We should expect that the effective phonon mode corresponds to some spectral feature, usually among the high-energy components of the vibrational spectra. An example in which 'pure' multiphonon relaxation is interpreted on the basis of a single, well-identified vibrational mode is the case of the non-radiative transitions from the $^4F_{9/2}$ state of Er^{3+} in CaSGG (see, for example, [15]).

The absorption and emission spectra and the decay kinetics of CaSGG doped with Er^{3+} have been reported in a previous paper [2]. In this crystal the optically-active species mainly substitute for the Ca^{2+} ions in sites with distorted dodecahedral symmetry. Emission bands from the $^4S_{3/2}$, $^4F_{9/2}$ and ^4I_J ($J = 9/2, 11/2$ and $13/2$) excited levels have been observed and the lifetimes of these states have been measured as a function of the temperature. In the case of luminescence from $^4S_{3/2}$, $^4I_{11/2}$ and $^4I_{13/2}$ levels there are different competing mechanisms occurring simultaneously which complicate the analysis of the decay data. Concerning the emission from the $^4F_{9/2}$ level, it has been outlined that its temperature dependence is typical of a multiphonon relaxation [2]; in the following we will give an analytical confirmation of this statement and evaluate the relation with the vibrational properties of the host lattice. The $^4F_{9/2} \rightarrow {}^4I_{15/2}$ emission band of CaSGG:Er^{3+} measured at 10 and 298 K with excitation at 514.5 nm is shown in figure 3. It can be noted that the number of optical features exceeds that expected on the basis of the crystal field splitting of the electronic states of Er^{3+}. This is due to the presence of different non-equivalent sites available for the optically-active ion, as discussed in [2]. Nevertheless, the decay curves of the luminescence are single exponential between 10 and 298 K. The Judd–Ofelt analysis of the room-temperature absorption spectrum allows one to evaluate a radiative lifetime of 103 μs for the $^4F_{9/2}$ emitting level. It is then possible to calculate the values of W_{NR} at different temperatures from (1). In this procedure, we assume that the radiative lifetime calculated using the Judd–Ofelt parameters is independent of the temperature.

Therefore, (2) can be used to reproduce the observed behaviour of W_{NR}. In figure 4 we report the results of the calculations performed considering third-, fourth- and fifth-order processes, phonon energies consistent with the gap between $^4F_{9/2}$ and the next-lower level, $^4I_{9/2}$ ($\sim$2650 cm^{-1}), and $W_{NR}^{(0)}$ obtained from the low-temperature data. It is evident that the experimental results are best reproduced by a fourth-order (i.e. $p = 4$) process with $W_{NR}^{(0)} = 18\,600$ s^{-1} and a phonon energy of about 660 cm^{-1}. Such a phonon corresponds

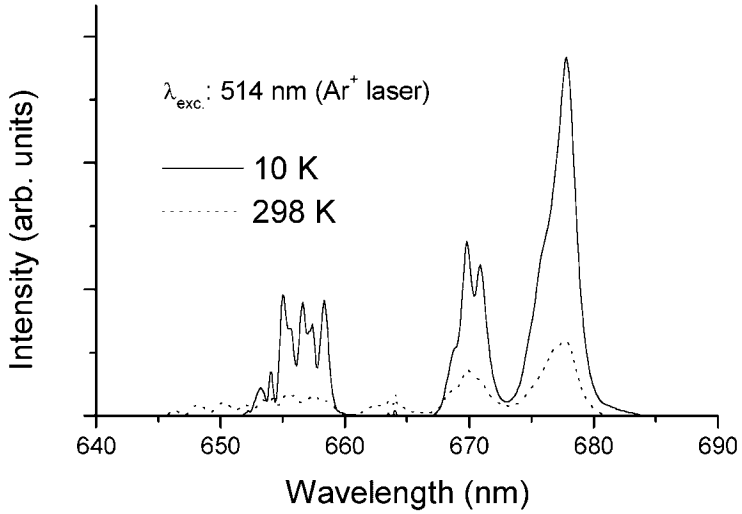

Figure 3. 10 and 298 K emission spectra of CaSGG:Er^{3+} in the 600–700 nm region. The transition involved is $^4F_{9/2} \rightarrow {}^4I_{15/2}$.

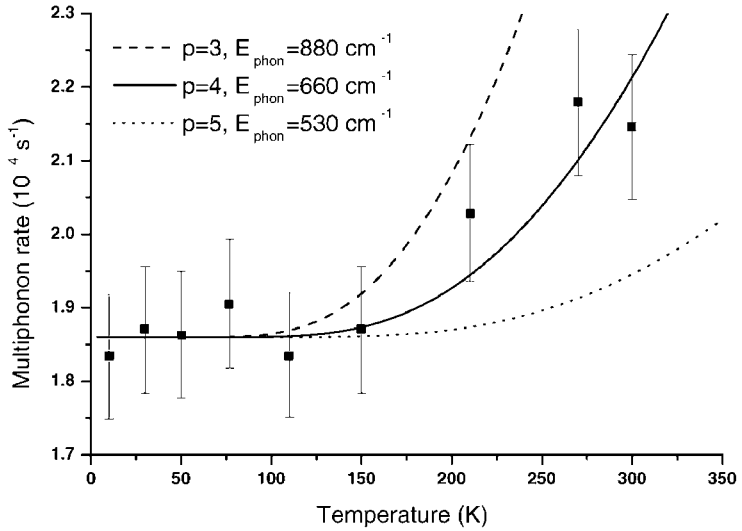

Figure 4. Temperature dependence of the non-radiative relaxation rate of the $^4F_{9/2}$ state of Er^{3+} in CaSGG.

approximately to bands present in the IR and Raman spectra and assigned to a ν_3 mode of the GeO_4^{4-} ion. The interaction of the electronic states of the rare earth ion with a mode assigned to the tetrahedral unit is not surprising: on one hand, equation (2) requires high-energy phonons to make the multiphonon relaxation process effective and, on the other hand, we have already observed that the dodecahedral groups share edges with the tetrahedral groups, and therefore their vibrational motions are strongly connected. The fact that the phonon energies involved in the other two processes do not find any correspondence in the vibrational spectra is, in our opinion, a confirmation of the reliability of the model.

4.2. Vibrational progressions in the optical bands of transition metal ions: the spectra of Cr^{3+} and Ni^{2+} in CaSGG

The radiative transitions between different electronic states of an optically-active ion in a vibrating lattice are usually discussed in the framework of the single configurational coordinate model (SCCM) [16]. The approximation of the model lies in the assumption that the electronic states are coupled with one representative mode only, and all the other modes are neglected. The transition probability between the vibrational level n of the electronic ground state a and the vibrational level m of the excited state b is then given by

$$W_{an-bm} = P_{ab}|\langle\chi_b(m) \mid \chi_a(n)\rangle|^2 \tag{4}$$

where P_{ab} is the purely electronic transition probability and $\chi_a(n)$, $\chi_b(m)$ are vibrational wavefunctions. The squares of their overlap integrals, $|\langle\chi_b(m) \mid \chi_a(n)\rangle|^2$, are known as the Franck–Condon factors. Their values are usually different from zero because the vibrational wavefunctions belong to different electronic states, with different equilibrium geometries. The evaluation of the Franck–Condon factors at $T = 0$ K leads to an absorption/emission band shape function of the type

$$I_{ab}(E) = I_0 \sum_m \frac{\exp(-S)S^m}{m!}\delta(E_0 \pm m\hbar\omega - E) \tag{5}$$

where I_0 is the intensity of the full band, S—the Huang–Rhys parameter, is a function of the difference in electron–phonon coupling between the ground and the excited states, the minus sign holds for emission and the plus sign for absorption transitions and $\hbar\omega$ is the frequency of the representative mode. If the optically-active ion does not form with the ligands' covalent bonds with a force constant that is too different with respect to the ions which have been substituted, this mode should find some correspondence in the IR or Raman spectrum of the compound under examination. Equation (5) can be used to fit the vibrational progressions observed in the electronic spectra. As S increases from zero (no-phonon lines plus sideband-type spectra) to large values (10–20, i.e. broadband spectra) the bands tend to broaden and to lose their vibrational structure; this is also because of the coupling with higher-energy modes. For this reason, the vibrational progressions can usually be observed for relatively low values of the parameter S [17].

The emission and absorption spectra of CaSGG:Cr^{3+} were reported and discussed in [1]. Figure 5 shows the high-energy side of the 10 K emission spectrum, recorded with excitation at 488 nm. This band is assigned to the $^4T_{2g} \rightarrow {}^4A_{2g}$ transition of the Cr^{3+} ion in an octahedral site. The corresponding absorption band also presents a mirror structure on its low-energy side. The fine structure can be assigned to a vibrational progression in two modes with energies of about 190–195 and 290–295 cm^{-1} superimposed on the origin of the magnetic dipole. A Huang–Rhys parameter $S \approx 4.4$, in agreement with the band shape, can be obtained using 295 cm^{-1} as a representative mode: this phonon energy corresponds to a mode (see table 1) present in the Raman spectrum.

In the case of CaSGG:Ni^{2+} [3], we have found a vibrational structure on the high-energy side of the $^3T_{1g} \rightarrow {}^3A_{2g}$ and $^1T_{2g} \rightarrow {}^3A_{2g}$ emission transitions of Ni^{2+} in octahedral sites (the latter is shown in figure 6), characterized by a progression in a phonon of 175–180 cm^{-1}, corresponding to lattice modes present in the Raman spectrum, as shown in table 1. Considering this value for the representative phonon mode, it is possible to calculate a Huang–Rhys factor of $S \approx 3.7$, which well accounts for the shapes of the magnetic dipole absorption and emission transitions between the ground state $^3A_{2g}$, and first excited state $^3T_{2g}$.

In this last case, it is evident that the vibrational mode involved in the progressions corresponds to lattice phonons. Moreover, it is interesting to note that both vibrational modes

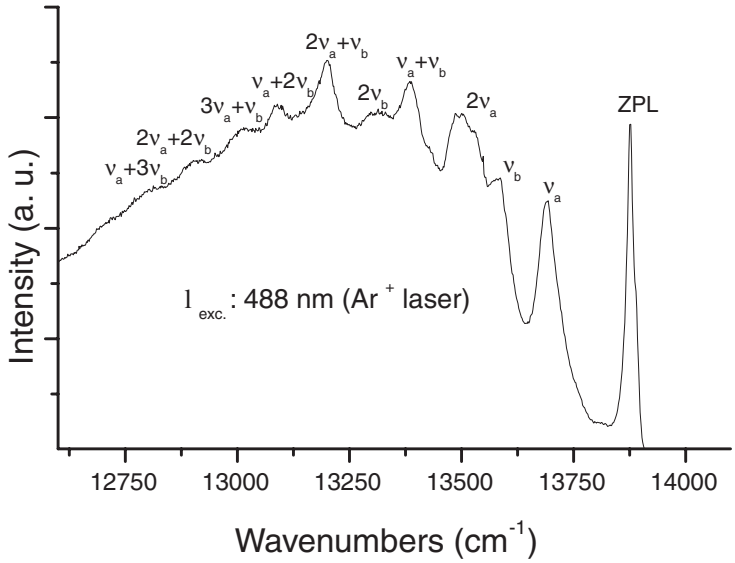

Figure 5. Vibrational progression in the low-energy side of the 10 K emission spectrum of CaSGG:Cr^{3+}. (ν_a = 190–195 cm^{-1} and ν_b = 290–295 cm^{-1}.)

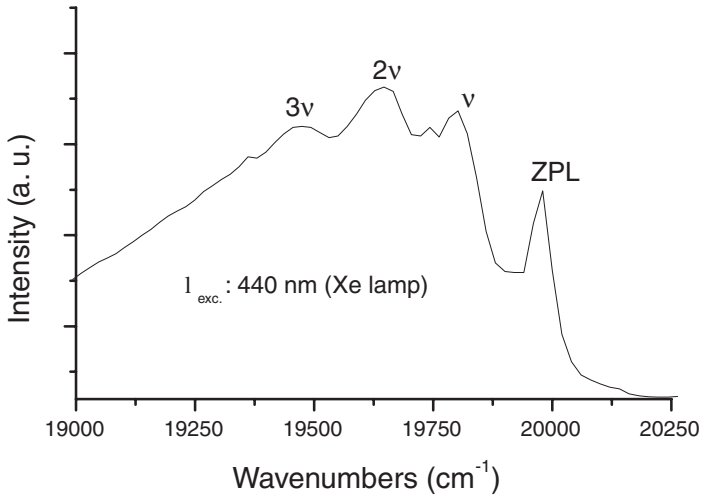

Figure 6. Vibrational progression in the low-energy side of the 10 K emission spectrum of CaSGG:Ni^{2+}. ($^1T_{2g} \rightarrow {}^3A_{2g}$ transition, ν = 175–180 cm^{-1}.)

at 180 and 295 cm^{-1} do not seem to be totally symmetric. This behaviour could be indicative of a Jahn–Teller coupling in the excited states [18].

5. Conclusions

We have measured the IR and Raman spectra of the garnet $Ca_3Sc_2Ge_3O_{12}$, which is a promising host lattice for luminescent ions. The spectral features were assigned in terms of internal and external modes of the tetrahedral GeO_4^{4-} moiety, and we have outlined the reasons why such

a model would deserve some improvement. We then took into consideration two aspects of the optical spectra of activated crystals, i.e. the multiphonon relaxation of the excited states of $4f^n$ ions and the vibrational structure of the low-temperature bands of $3d^n$ ions. We have shown that there is a good correspondence between the vibrational information contained in the IR, Raman and electronic spectra. It has to be noted that the substitution of a dopant ion for a lattice constituent leads to a local perturbation, due to different metal–oxygen bond strengths and to the different masses of the dopants. It is obvious that such a perturbation can only weakly affect the IR or the Raman spectra of the crystal, especially if the doping level is low. In contrast, the electronic spectra are induced by the presence of the optically-active ion, and then they should strongly depend on the local interactions between the dopant and its neighbourhood. The good correspondence between the phonon energies involved in the electronic transitions and the vibrational modes observed in the IR or Raman spectra seems to demonstrate that the local perturbation effects due to the accommodation of small amounts of dopant ions are, in the present case, relatively small. This point is of importance because it allows one to refer to the vibrational spectra to discuss the possible mechanisms depending on the ion–lattice interactions.

Acknowledgments

The authors thank Erica Viviani (University of Verona) for technical assistance. This work was carried out with the financial contributions of MURST ('Ministero dell'Università e della Ricerca Scientifica e Tecnologica'—Research project year 1997 prot. 9703105065) and CNR ('Consiglio Nazionale delle Ricerche'—PF MSTA II 97.00924.PF34).

References

[1] Cavalli E, Zannoni E and Belletti A 1996 *Opt. Mater.* **6** 153
[2] Comini E, Toncelli A, Tonelli M, Zannoni E, Cavalli E, Speghini A and Bettinelli M 1997 *J. Opt. Soc. Am.* B **14** 1938
[3] Zannoni E, Cavalli E, Toncelli A, Tonelli M and Bettinelli M 1999 *J. Phys. Chem. Solids* **60** 449
[4] Cavalli E, Zannoni E, Belletti A, Carozzo V, Toncelli A, Tonelli M and Bettinelli M 1999 *Appl. Phys.* B **68** 677
[5] Mill B V 1975 *Sov. Phys. Cryst.* **19** 3595
[6] Hurrell J P, Porto S P S, Chang I F, Mitra S S and Bauman R P 1968 *Phys. Rev.* **173** 851
[7] McDevitt N T 1969 *J. Opt. Soc. Am.* **59** 1240
[8] Tarte P 1967 *Spectrochim. Acta* A **23** 2127
[9] Koningstein J A and Sonnich Mortensen O 1968 *J. Mol. Spectrosc.* **27** 343
[10] Nakamoto K 1997 *Infrared and Raman Spectra of Inorganic and Coordination Compounds* (New York: Wiley) p 198
[11] Kaminskii A A 1996 *Crystalline Lasers: Physical Processes and Operating Schemes* (Boca Raton, FL: CRC Press) p 307
[12] Kaminskii A A 1996 *Crystalline Lasers: Physical Processes and Operating Schemes* (Boca Raton, FL: CRC Press) p 227
[13] Ofelt G S 1962 *J. Chem. Phys.* **37** 511
[14] Judd B R 1962 *Phys. Rev.* **127** 750
[15] Flaherty J M and DiBartolo B 1975 *J. Lumin.* **8** 51
[16] Henderson B and Imbusch G F 1989 *Optical Spectroscopy of Inorganic Solids* (Oxford: Clarendon) p 197
[17] Henderson B and Imbusch G F 1989 *Optical Spectroscopy of Inorganic Solids* (Oxford: Clarendon) p 201
[18] Güdel H U and Snellgrove T R 1978 *Inorg. Chem.* **17** 1617